

Non-Markovian environment induced Schrödinger cat state transfer in an optical Newton's cradle

XINYU ZHAO AND YAN XIA*

Fujian Key Laboratory of Quantum Information and Quantum Optics (Fuzhou University), Fuzhou 350116, China

Department of Physics, Fuzhou University, Fuzhou 350116, China

**xia-208@163.com*

Abstract: In this manuscript, we study the Schrödinger cat state transfer in a quantum optical version of Newton's cradle in non-Markovian environment. Based on a non-Markovian master equation, we show that the cat state can be transferred purely through the memory effect of the non-Markovian common environment, even without any direct couplings between neighbor cavities. The mechanism of the environment induced cat state transfer is analyzed both analytically and numerically to demonstrate that the transfer is a unique phenomenon in non-Markovian regime. From this example, the non-Markovian environment is shown to be qualitatively different from the Markovian environment reflected by the finite versus zero residue coherence. Besides, we also show the influence of environmental parameters are crucial for the transfer. We hope the cat state transfer studied in this work may shed more light on the fundamental difference between non-Markovian and Markovian environments.

1. Introduction

Schrödinger cat state [1, 2] is a fundamental topic in quantum mechanics since it may reveal the boundary between the quantum and the classical realms as well as the transition from one to the other [3–8]. As a result, cat state has attracted a lot of research interest [9–16], various theoretical and experimental studies are made to observe such a superposition state. So far, a lot of analogs of Schrödinger cat states have been demonstrated experimentally in optical system [10, 17–21], atomic system [9], magnon system [12, 22], solid state system [23–25], and many other systems [24, 26], even including bio-organic systems [26].

The investigations on Schrödinger cat state are not only crucial for testing fundamental concepts of quantum mechanics, but also valuable for applications in quantum computing [17–21, 27–38]. For example, cat states are utilized for encoding quantum information and correcting quantum errors [19, 27, 29, 39]. Fault tolerant quantum computation based on cat state qubit [19, 40, 41] shows huge potential of beating the break-even point of quantum error correction [42]. At the application level, besides the cat state preparation [43–45], the transfer of Schrödinger cat state could be equally important [46–49]. Because in a quantum processor, the information has to be transported from one processing unit to another frequently, so the cat state as the information carrier must be faithfully transferred without losing its coherence [50, 51]. Therefore, a large amount of research has also been focused on the coherent transfer of cat state in various physical systems. For example, in Ref. [47], the authors investigate the cat state transfer from a microscopic system to a macroscopic system. In Ref. [52], the authors investigate the cat state swapping in optomechanical system. In Ref. [24], the authors study the cat state transfer between a cavity and a solid state quantum-dot system. However, in all of these physical systems, the research often focus on the cat state transfer caused by the couplings inside quantum systems. The cat state transfer purely caused by the non-Markovian environments has not received enough attention.

In this manuscript, we study the cat state transfer in an optical analog of Newton's cradle [53] embedded in a non-Markovian common environment as shown in Fig. 1. Beyond the existing literature [24, 46–49, 52, 54–57], our focus is not the transfer induced by the direct couplings

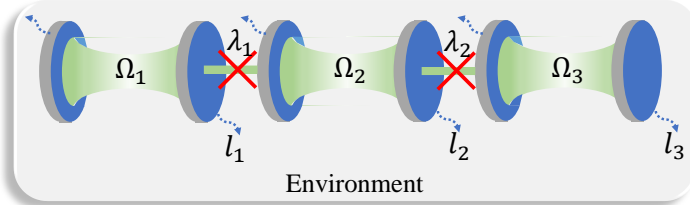


Fig. 1. Schematic diagram of a coupled N -cavity array (a quantum optical analog of the classical Newton's cradle [53]) interacting with a common environment. In this manuscript, we mainly focus on the “no direct coupling” case $\lambda_i = 0$.

between cavities [53], but the transfer purely induced by the non-Markovian environment. Analog to the classical Newton's cradle composed of several identical balls [58–60], our research is separating the balls and investigate the energy transfer between the balls through the air resistance. The analytical results prove that the cat state can indeed transfer purely through environment, and this is a unique phenomenon in non-Markovian regime showing the fundamental difference between Markovian and non-Markovian environments. Besides, the properties of the environment [61–66] is proved to be crucial for the transfer.

To be specific, we first derive the dynamical equations governing the evolution of the cavity array system in non-Markovian case. Then, based on these equations, we numerically study the influence of the memory time of the environment. By monitoring the fidelity and the Wigner function of the transferred cat state, we point out that the cat state will be transferred faithfully only in non-Markovian case when there are no directly couplings. As a comparison, the transferred state will lose all the coherence in Markovian case. The mechanism of environment induced transfer is investigated analytically, and the numerical results also confirm this phenomenon only exists in non-Markovian case.

The environment induced cat state transfer reveals that the difference between non-Markovian and Markovian environment is qualitative (finite or zero residue coherence) other than quantitative (strong or weak residue coherence). A simple and straightforward example is that the weak but non-zero residue coherence in non-Markovian case keeps the possibility for future distillation [67, 68]. Last but not least, we investigate how to transfer the cat state into a desired cavity by manipulating the coupling strengths between cavities. By tuning the coupling strengths, one can transfer the cat state into a particular cavity.

2. Optical Newton's cradle in non-Markovian environment

2.1. Quantum mechanical description of optical Newton's cradle

We consider a coupled cavity array (a quantum version of Newton's cradle [53]) interacting with a non-Markovian common environment as shown in Fig. 1. The Hamiltonian of such a system can be described by

$$H = H_S + H_B + H_{\text{int}}, \quad (1)$$

with the Hamiltonian of the cavity array system [69–72]

$$H_S = \sum_{i=1}^N \Omega_i a_i^\dagger a_i + \sum_{i=1}^N \lambda_i (a_i^\dagger a_{i+1} + a_i a_{i+1}^\dagger), \quad (2)$$

where Ω_i ($i = 1, 2, \dots, N$) are the eigen-frequencies for each cavity in the array, and λ_i are the coupling strengths between i^{th} cavity and $(i+1)^{\text{th}}$ cavity. An open boundary condition is chosen here, namely the first and the last cavity form two open ends ($\lambda_N = 0$).

The Hamiltonian in Eq. (2) actually represents a huge category of quantum system not limited to “cavities”. For example, wave-guide system [53], LC oscillator in superconducting circuits [73] and many other bosonic systems modeled by quantum harmonic oscillators [74] can be also interpreted as H_S . Here, we use cavity array as an example to present our study, but the conclusion should apply to all similar systems.

We assume that all the cavities are coupled to a bosonic common environment

$$H_B = \sum_j \omega_j b_j^\dagger b_j, \quad (3)$$

where b_j are the annihilation operator of the j^{th} mode. The interaction Hamiltonian between the system and the environment under rotating wave approximation can be formally written as

$$H_{\text{int}} = \sum_j (g_j b_j^\dagger A + g_j^* b_j A^\dagger), \quad (4)$$

where the operator $A = \sum_{i=1}^N l_i a_i$ represents a collective coupling operator between the environment and all the cavities. For simplicity, l_i are always set to be 1, except in the discussion in Sec. 5.

2.2. Derivation of dynamical equations

By using the coherent state $|z\rangle = \otimes \prod_j |z_j\rangle$ representation of the environment, one can define a stochastic state vector $|\psi(t, z)\rangle \equiv \langle z|\psi_{\text{tot}}(t)\rangle$ living in the Hilbert space of the system only. Here, $|\psi_{\text{tot}}(t)\rangle$ is the total state vector describing the state of system plus environment, and $|z\rangle$ is a collective coherent state of all the environmental modes, whose j^{th} mode is in the coherent state $|z_j\rangle$. Based on the fact that the total state vector $|\psi_{\text{tot}}(t)\rangle$ should satisfy the Schrödinger equation $\frac{d}{dt}|\psi_{\text{tot}}(t)\rangle = -iH_I|\psi_{\text{tot}}(t)\rangle$ (H_I is the Hamiltonian in the interaction picture and we set $\hbar = 1$ here and throughout the paper), the stochastic state vector should satisfy the following dynamical equation called non-Markovian quantum state diffusion (NMQSD) equation [75–85],

$$\frac{\partial}{\partial t}|\psi(t, z)\rangle = \left[-iH_S + Az_t^* - A^\dagger \int_0^t ds K(t, s) \frac{\delta}{\delta z_s^*} \right] |\psi(t, z)\rangle, \quad (5)$$

where $K(t, s) = \sum_j |g_j|^2 e^{-i\omega_j(t-s)}$ is the correlation function, and $z_t^* = -i \sum_j g_j z_j^* e^{i\omega_j t}$ is a complex stochastic noise satisfying $M[z_t] = M[z_t z_s] = 0$, $M[z_t^* z_s] = K(t, s)$. Here $M[\cdot] \equiv \int \frac{dz^2}{\pi} e^{-|z|^2} [\cdot]$ denotes the statistical average over the noise z_t^* . If we define the environment operator as $B(t) = \sum_j g_j^* b_j e^{-i\omega_j t}$, the correlation function can be also interpreted as

$$K(t, s) = \langle B(t) B^\dagger(s) \rangle = \sum_j |g_j|^2 e^{-i\omega_j(t-s)}, \quad (6)$$

where the summation over j can be replaced by an integral over the frequency ω as $K(t, s) = \int_0^\infty d\omega g(\omega) e^{-i\omega(t-s)}$. The distribution function $g(\omega)$ is called the spectrum density of the environment.

In order to solve Eq. (5), we replace the functional derivative $\frac{\delta}{\delta z_s^*}$ by an operator $O(t, s, z^*)$ as,

$$\frac{\delta}{\delta z_s^*} |\psi(t, z)\rangle = O(t, s, z^*) |\psi(t, z)\rangle. \quad (7)$$

Then, Eq. (5) can be rewritten as

$$\frac{\partial}{\partial t} |\psi(t, z)\rangle = \left[-iH_S + Az_t^* - A^\dagger \bar{O}(t, z^*) \right] |\psi(t, z)\rangle, \quad (8)$$

where $\bar{O}(t, z^*) \equiv \int_0^t ds K(t, s) O(t, s, z^*)$ and the initial condition $O(t, s = t, z^*) = A$ should be satisfied. Here, the operator O is replaced by a formally time-local operator \bar{O} , which is a time integration over all the time points s ($s \leq t$). The impact of the evolution history (non-Markovian effect) is reflected in this time-domain convolution.

Now, the key to solving the dynamic equation (8) is the operator O . According to the consistency condition $\frac{\delta}{\delta z_s} \frac{\partial}{\partial t} |\psi(t, z)\rangle = \frac{\partial}{\partial t} \frac{\delta}{\delta z_s} |\psi(t, z)\rangle$ [76, 78], O should satisfy the equation

$$\frac{\partial}{\partial t} O = [-iH_S + Az_t^* - A^\dagger \bar{O}, O] - A^\dagger \frac{\delta}{\delta z_s} \bar{O}. \quad (9)$$

From Eq. (9), the exact O operator of this model can be derived as

$$O(t, s) = \sum_{i=1}^N f_i(t, s) a_i, \quad (10)$$

where $f_i(t, s)$ are time-dependent coefficients satisfying the following equations,

$$\frac{\partial}{\partial t} f_i(t, s) = i\Omega_i f_i(t, s) + i[\lambda_i f_{i+1}(t, s) + \lambda_{i-1} f_{i-1}(t, s)] + \sum_{j=1}^N f_j(t, s) F_i(t), \quad (11)$$

and $F_i(t) = \int_0^t ds K(t, s) f_i(t, s)$ ($i = 1, 2, \dots, N$), with the initial conditions

$$f_i(t = s, s) = 1. \quad (12)$$

With the exact solution of operator O in Eq. (10), one can numerically simulate Eq. (8) to obtain the reduced density operator of the system by taking the statistical average over the stochastic wave function $|\psi(t, z)\rangle$ as

$$\rho(t) = M[|\psi(t, z)\rangle\langle\psi(t, z)|] = \int \frac{dz^2}{\pi} e^{-|z|^2} |\psi(t, z)\rangle\langle\psi(t, z)|. \quad (13)$$

Alternatively, one can also derive the corresponding master equation from Eq. (13) by taking time-derivative on both sides. Then, using the Novikov theorem [78, 80], one can obtain the following master equation

$$\frac{d}{dt} \rho = -i [H_S, \rho] + \left\{ \sum_k F_k(t) [A, \rho a_k^\dagger] + h.c. \right\}. \quad (14)$$

We would like to emphasize that the NMQSD equation (5), as well as the master equation (8), are derived directly from the microscopic Hamiltonian (1) without any approximation. The detailed derivation is presented in Appendix A. It is the exact dynamical equation governing the dynamics of the cavity array coupled to the environment, particularly in the non-Markovian regime. This method has been widely studied and used in various physical systems [86–96].

In the derivation above, we assume the temperature is zero, i.e., the initial state of the environment is the vacuum state. However, the finite temperature case only slightly increase the complexity of the equations without changing the physical performance we focused on (see discussion in Sec. 3). In Appendix B, the NMQSD equation and the master equation for finite temperature case are derived.

2.3. Spectrum density and correlation function of the environment

The environmental impact on the dynamics of the optical Newton’s cradle is reflected on the terms Az_t^* and $-A^\dagger \bar{O}$ in Eq. (8). If these two terms are zero, the equation is reduced to

$\partial_t |\psi(t, z)\rangle = -iH_S |\psi(t, z)\rangle$, which is the Schrödinger equation for the closed system. The non-Markovian properties are reflected by the correlation function $K(t, s)$ in Eq. (5) through the time-domain convolution in \bar{O} . An evolution without memory effect will be represented by a δ -type correlation function as $K(t, s) = \Gamma\delta(t, s)$, which means the evolution at time point “ t ” is independent of the behavior at any previous time point “ s ”. As a result, the operator \bar{O} is reduced to $\bar{O} = \frac{\Gamma}{2}A$ due to the initial condition $O(t = s, s, z^*) = A$. Then, Eq. (8) is reduced to the commonly used Markovian quantum trajectory equation [97, 98], and Eq. (14) is reduced to the standard Lindblad master equation [78] with constant coefficients.

The results presented here are independent of a specific form of the correlation functions $K(t, s)$. Therefore, Eq. (8) and Eq. (14) are applicable to arbitrary correlation functions. One can definitely use any correlation function either predicted from microscopic models or directly measured from experiments. However, in the numerical simulation in Sec. 3, we choose the Lorentzian spectrum density

$$g(\omega) = \frac{\Gamma\gamma^2/2\pi}{(\omega - \Delta)^2 + \gamma^2}, \quad (15)$$

corresponding to the Ornstein-Uhlenbeck (O-U) type correlation function

$$K(t, s) = \frac{\Gamma\gamma}{2} e^{-(\gamma+i\Delta)|t-s|}. \quad (16)$$

In Eq. (15) and (16), the parameter $\tau = 1/\gamma$ indicates the memory time of the environment, Δ is the central frequency of the environment, and Γ is a global dissipation rate. The Lorentzian spectrum density of the environment has been widely used in the research on optical systems [79, 82, 99] and other systems [80, 100, 101]. The reason we choose O-U correlation function is because it is easy to observe the transition from non-Markovian regime to Markovian regime. If the memory time $\tau = 1/\gamma$ is very small in Eq. (16), $K(t, s)$ is approximately reduced to $K(t, s) \approx \Gamma\delta(t, s)$, which means the environment is reduced to a Markovian environment.

It is worth to note the NMQSD equation and master equation derived in this paper are applicable to arbitrary noises. The procedure of numerically generating arbitrary noises can be found in Ref. [96].

2.4. Numerical methods: Pure state trajectories and master equation

To numerically study the dynamics of the optical Newton’s cradle, one can either simulate Eq. (8) and Eq. (14). Both of them will produce identical results [78]. However, for a multipartite continuous variable system like the cavity array, simulating the density operator ρ is more difficult than simulating the pure state vector $|\psi(t, z)\rangle$. Since the cat state is not a Gaussian state, we should use a cut-off N_c on the Fock basis to a certain photon number N_c for each cavity. The memory usage for storing a state vector containing three cavities is $\sim N_c^3$, but the memory usage of storing a density operator is $\sim N_c^6$. Besides, the non-Markovian effect make all the time points “ s ” in the history may have a potential contribution. If the time evolution is divided into 1000 steps, the total memory consumption for density operator approach is at least $1000N_c^6$. For $N_c = 10$ which is far below the precision requirements for simulating coherent states, the memory usage for storing a single density operator is 1 Gigabytes. For $N_c = 20$ which can provide a moderate precision, the usage dramatically increases to 64 Gigabytes, which is far beyond a typical desktop computer. As a comparison, the memory usage for state vector is only about $1000N_c^3$ (about 8 Megabytes). Although the discussion above is merely a rough estimation of the memory usage, one can conclude that the NMQSD equation (8) has a great computational advantage.

Although the master equation lose the competition in numerical simulation, it has its own advantages. Unlike the stochastic state vector that has an unclear and controversial physical interpretation [102, 103], the physical meaning of density operator is clear. Therefore, the master

equation is helpful for analytical investigation of the physical process. In Sec. 4, the mechanism of environment induced cat state transfer is just revealed by analyzing the master equation. In summary, Eq. (8) and Eq. (14) have their own advantages, so we have derived both equations and utilize their strengths in different scenarios.

3. Environment induced cat state transfer

In this section, we will focus on the cat state transfer based on the non-Markovian dynamical equations derived in Sec. 2. We assume the initial state of the 1st cavity is prepared in a superposition of two coherent states $|\alpha\rangle$ and $|-\alpha\rangle$, i.e., the cat state

$$|\psi_{\text{cat}}\rangle = 1/\sqrt{N}(|\alpha\rangle + |-\alpha\rangle), \quad (17)$$

where N is a normalization factor. The other two cavities are in the vacuum state, i.e., $|\psi(0)\rangle = |\psi_{\text{cat}}\rangle_1 \otimes |0\rangle_2 \otimes |0\rangle_3 \otimes \cdots \otimes |0\rangle_N$. The fidelity \mathcal{F}_i is used to quantify the performance of the cat state transfer. Since the cat state may rotate in time evolution, so all the rotated cat state $|\psi_{\text{cat}}^{(R)}(\theta)\rangle = 1/\sqrt{N}(|\alpha e^{-i\theta}\rangle + |-\alpha e^{-i\theta}\rangle)$ with a dynamical phase angle θ can be considered as a successful transfer of the cat state. Therefore, we define the fidelity of the transferred state as

$$\mathcal{F}_i = \max_{\{\theta\}} [\langle \psi_{\text{cat}}^{(R)}(\theta) | \rho_i(t) | \psi_{\text{cat}}^{(R)}(\theta) \rangle] \quad (i = 2 \text{ to } N), \quad (18)$$

where $\rho_i(t)$ are the reduced density matrices for the i^{th} cavity, and the fidelity is defined as the maximum fidelity between $\rho_i(t)$ and $|\psi_{\text{cat}}^{(R)}(\theta)\rangle$ over all possible phase factor θ .

3.1. Memory effect

It is not surprising that the cat state can be transferred when the couplings between neighboring cavities are finite ($\lambda_i > 0$) [53]. In this manuscript, the most interesting result is that a high fidelity cat state transfer can be still achieved without direct couplings ($\lambda_i = 0$ for all i). We first consider a simple case with only two coupled cavities ($N = 2$). In Fig. 2, the time evolution of the fidelity \mathcal{F}_2 is plotted as a function of the memory time $\tau = 1/\gamma$. When the memory time is sufficiently long (τ is large), it is clear that the cat state has been successfully transferred into the other cavity with a high fidelity $\mathcal{F}_2 \approx 1$. Since the direct coupling is absent, the common environment is the only connection among cavities. Therefore, such a cat state transfer is purely induced by the non-Markovian environment. In this sense, the non-Markovian properties of the environment must be essential to the fidelity of the transfer. From Fig. 2 (a), the fidelity of the transfer \mathcal{F}_2 decreases when the memory time τ decreases, which implies the high fidelity transfer only occurs in non-Markovian regime.

A deeper investigation shows that the cat state transfer in Markovian and non-Markovian regimes can be fundamentally different. To show this difference, we select several peaks (the maximum \mathcal{F}_2 can be achieved for given τ) in Fig. 2 (a) and plot the Wigner functions of the transferred state in subplots (b) to (g). The Wigner function is another indicator to quantify the performance of the transfer, because the residue quantum coherence (superposition) can be reflected by the negative region in the Wigner functions. In Fig. 2 (b), the interference fringe is clear indicating the coherence is maintained perfectly. This is also confirmed by the high fidelity $\mathcal{F}_2 \approx 1$. As a comparison, in Fig. 2 (g), the negative region disappears which means a complete loss of quantum coherence after the transfer. Although the fidelity is still finite $\mathcal{F}_2 > 0$, the quantum information encoded in the cat state is completely lost and only classical information is left. The subplots (b) to (g) just show the transition that coherence is gradually lost when the environment is changing from non-Markovian to Markovian.

It is worth to note that the physics revealed in the Wigner functions in Fig. 2 (b) to (g) is far beyond the information reflected by the fidelity in Fig. 2 (a). The Wigner functions show

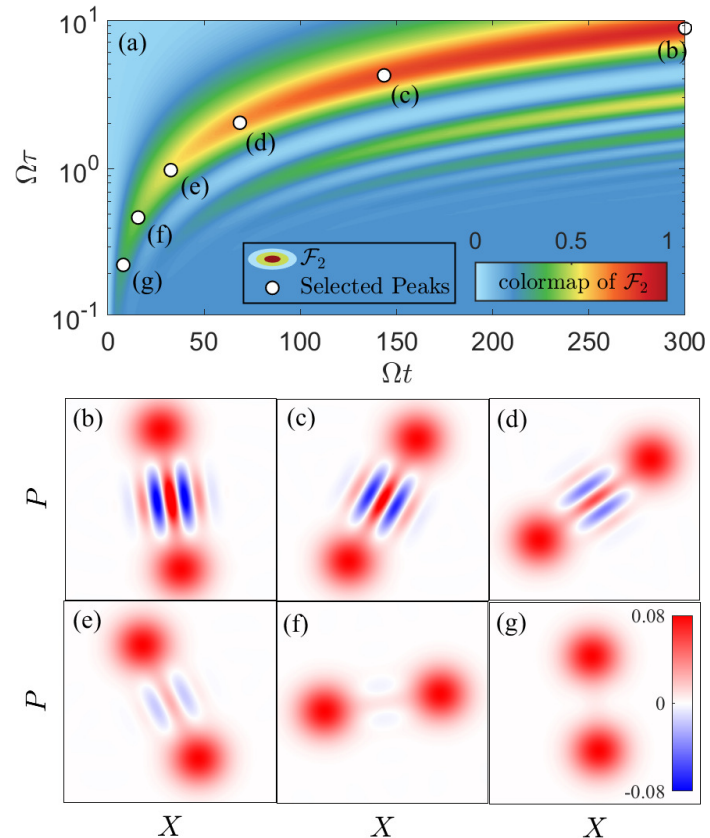


Fig. 2. Cat state transfer in two cavities ($N = 2$) without direct couplings ($\lambda_i = 0$). (a) Time evolution of the transferred fidelity \mathcal{F}_2 . The transition from Markovian to non-Markovian regime is reflected by the increasing τ in the y-axis. (b)-(g) are the Wigner functions at the positions pointed by the markers in (a), respectively. The initial size of the cat state is $\alpha = 2$. The other parameters are $\Omega_1 = \Omega_2 = \Omega = 1$, $\Delta = 10$, $\Gamma = 1$.

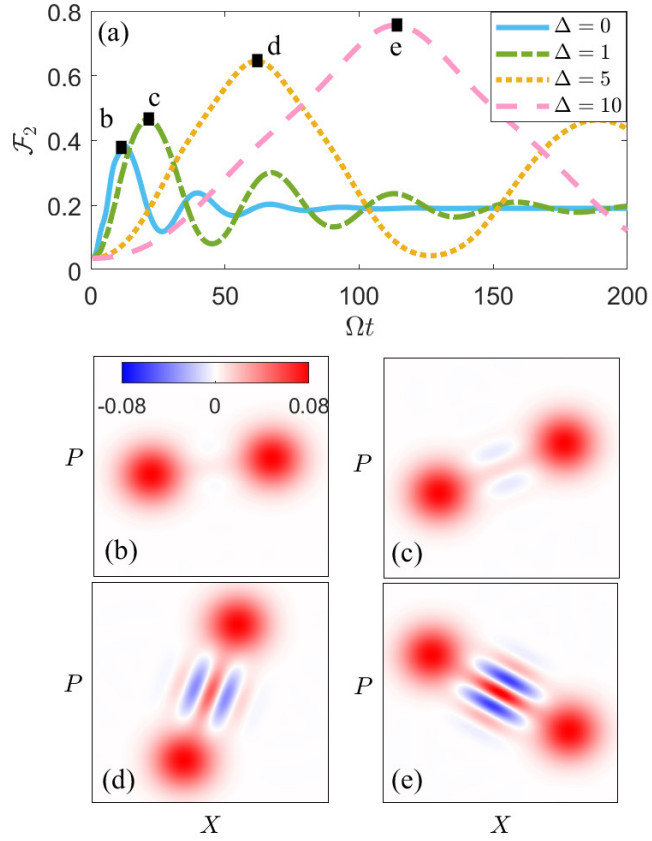


Fig. 3. Influence of the central frequency Δ of the environmental density spectrum. (a) Time evolution of the transferred fidelity \mathcal{F}_2 . (b) to (e) are the Wigner functions at the positions pointed by the markers in (a). The parameters are $\alpha = 2$, $\gamma = 0.3$, $\Omega_1 = \Omega_2 = \Omega = 1$, $\lambda_i = 0$, $\Gamma = 1$.

that the influence of the environment can be qualitative (zero or finite residue coherence) other than quantitative (low or high fidelity). Similar topics are widely discussed in the research on entanglement sudden death versus asymptotic decay [67, 104]. Despite the comprehensive discussion on the fundamental concepts in quantum mechanics [68], an apparent difference between zero residue coherence and weak but finite residue coherence is that the latter case still keeps the possibility for distillation schemes.

3.2. Central frequency of the spectrum density

Besides the memory time τ discussed in Sec. 3.1, the central frequency Δ is another important environmental parameter which is crucial for the environment induced cat state transfer. In Fig. 3, a higher central frequency Δ leads to a larger maximum fidelity \mathcal{F}_2 , but the evolution time to achieve maximum \mathcal{F}_2 also becomes longer. Similar to Fig. 2, the phenomenon that the residue coherence is completely lost also appears in Fig. 3. When Δ is smaller than a certain threshold, the negative region in the Wigner functions disappears as shown in Fig. 3 (b). This reveals that long memory time τ is not a sufficient condition to avoid complete loss of coherence. Even in the case τ is large enough (as shown in Fig. 3, $\gamma = 0.3$ or $\tau = 1/\gamma \approx 3.33$), coherence can be

completely lost in small Δ case. Both proper τ and Δ are only necessary conditions to achieve a successful transfer.

In this section, we focus on the case without direct couplings ($\lambda_i = 0$). The properties of the environment such as τ and Δ are naturally important, since the transfer is purely induced by the environment. Actually, in the case with direct couplings ($\lambda_i > 0$), these environmental parameters are also crucial for the cat state transfer. In Sec. 6, we show the non-Markovian effect can significantly enhance the transfer and cause the revival of the transferred coherence in certain conditions.

4. Mechanism of environment induced transfer

The mechanism of the cat state transfer can be revealed by analyzing the master equation (14). In the case $\lambda_i = 0$, the first term in Eq. (14) only contains free rotations $-i \sum_{i=1}^N \Omega_i [a_i^\dagger a_i, \rho]$ but no interactions between cavities. The indirect interactions between cavities only originate from the terms $\sum_k F_k(t) [A, \rho a_k^\dagger] + h.c.$. In the two-cavity case, the coefficients F_1 and F_2 are identical since both the differential equations in (11) and the boundary conditions in (12) are symmetric for F_1 and F_2 . Therefore, the coefficients can be simplified as $F_1 = F_2 = F$ in the symmetric case, leading to the master equation contains the following indirect interaction term

$$2\Im(F) \left\{ -i \left[\rho, a_1^\dagger a_2 + a_2^\dagger a_1 \right] \right\}, \quad (19)$$

where $\Im(F)$ indicates the imaginary part of the coefficient F . If we define $H_{\text{eff}} = a_1^\dagger a_2 + a_2^\dagger a_1$, this term can be further written as $2i\Im(F) [H_{\text{eff}}, \rho]$. It is clear that the contribution of Eq. (19) in the master equation is equivalent to a direct interaction term in the Hamiltonian in Eq. (2). The only difference is the former one originates from the impact of the environment and later one originates from the direct interaction in the system Hamiltonian. It is well known that the Hamiltonian in the form $H_{\text{eff}} = a_1^\dagger a_2 + a_2^\dagger a_1$ (in mathematical perspective, no matter direct or indirect) will cause a quantum state transfer. This has been widely proved in either previous papers [46–48] or the numerical results in Sec. 6. Therefore, the $\Im(F)$ term in Eq. (19) will cause a quantum state transfer as if there is a direct interaction in the system Hamiltonian.

While the imaginary part $\Im(F)$ leads to an indirect coupling, the real part $\Re(F)$ corresponds to the traditional dissipation effect which is similar to the widely studied dissipation term in Lindblad master equation. The cat state transfer is a combined effect of both $\Re(F)$ and $\Im(F)$. In Fig. 4, the long-time behavior of $\Re(F)$ and $\Im(F)$ are plotted. The ratio $\Im(F)/\Re(F)$ somehow reflects which effect is dominant, the dissipation or the indirect coupling. The numerical results imply that a successful cat state transfer prefers larger τ and larger Δ . This is consistent with the results shown in Fig. 2 and Fig. 3.

It is worth to note that the $\Im(F)$ term in Eq. (19) only exists in non-Markovian case. One can check that $F_1(t) = F_2(t) = \Gamma/2$ when $K(t, s) = \Gamma\delta(t, s)$ in a straightforward manner. Namely, in Markovian case, the δ -type correlation function results in $\Im(F_1) = \Im(F_2) = 0$ and the master equation is reduced to the Lindblad form [78]. In another word, non-Markovian correlation function is a necessary condition to produce the indirect interaction in Eq. (19). From this point of view, we have mathematically proved that the environment induced cat state transfer is a purely non-Markovian phenomenon. This also explains why the cat state can not be transferred in weak Markovian case as shown in Fig. 2 (g), because the indirect interaction $\Im(F)$ is too weak to fight against the dissipation $\Re(F)$. Quantum coherence is completely lost before it is transferred. Again, this is qualitatively different from quantitative impact of the environment.

Last but not least, we would like to emphasize that in the finite temperature case, the conclusion that environment induced transfer is purely a non-Markovian phenomenon still holds. Similar to the case in zero temperature case, the coefficients in the \hat{O} operator become constant real numbers. For more details, see the derivation in Appendix B.

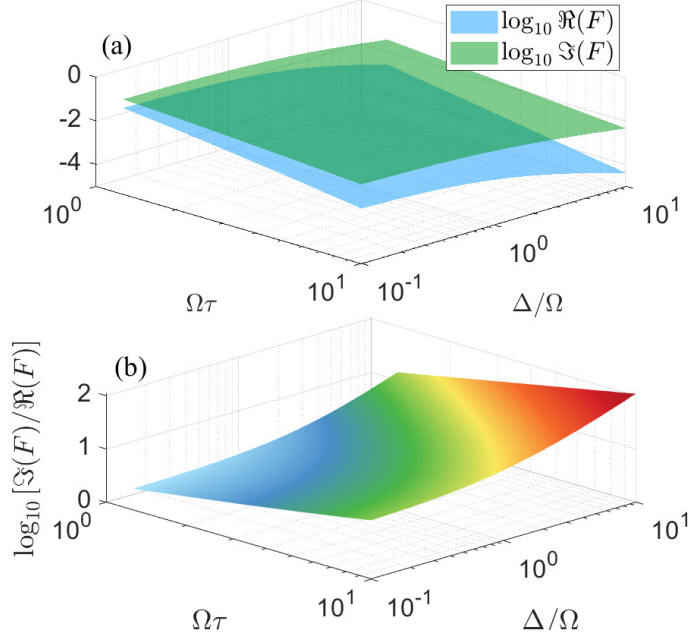


Fig. 4. Non-Markovian impact on the long-term ($t \approx \infty$) behavior of the coefficient F . The real and imaginary part of F are plotted in (a) with environmental parameters Δ and τ . (b) The ratio of $\Im(F)/\Re(F)$.

5. Environment induced cat state transfer in multiple cavities

In Sec. 3, we only show the two-cavity case ($N = 2$) as an example. In this section, we will focus on the case that multiple cavities are coupled to the environment. Taking three-cavity case ($N = 3$) as an example, the 2nd and 3rd cavities are in the symmetric positions. Due to this symmetric property in Eq. (14) as well as in its initial conditions, the solution of $\rho^{(2)}(t)$ will be identical to $\rho^{(3)}(t)$. In order to transfer the cat state into a desired cavity purely through the assistance of environment, the coupling strengths to the environment l_1 , l_2 , and l_3 must be different. Here, we assume $l_1 = 1$, $l_2 = 1 - \delta l$, and $l_3 = 1 + \delta l$, where δl describes the difference of the coupling strengths between the 2nd and 3rd cavities. An asymmetric parameter can be defined as

$$\eta = \frac{l_3 - l_2}{l_2 + l_3}, \quad (20)$$

to measure the asymmetry of the two coupling strengths l_2 and l_3 .

It is straightforward to draw a conclusion for the two limiting cases $\eta = -1$ and $\eta = 1$. For $\eta = -1$, $l_3 = 0$, the model is reduced into $N = 2$ case discussed in Sec. 3, because the 3rd cavity is decoupled from the environment thus losing all the connections to other cavities (no direct coupling $\lambda_i = 0$). Similarly, in the case $\eta = 1$, the 2nd cavity is decoupled. One may expect that a high-fidelity transfer to the 3rd cavity needs $\eta \approx 1$ or $\delta l \approx 1$ to almost fully decouple the 2nd cavity. However, the numerical results in Fig. 5 show a mild asymmetry can just ensure a high-fidelity transfer. The pink marker in the main plot shows that a high fidelity $\mathcal{F}_3 \approx 0.9$ can be achieved for $\eta = 0.5$, i.e., $\delta l = 0.5$, far from the limiting case $\eta = 1$. Besides, the fidelity increase rapidly with the increase of η . So, a decent transfer can be achieved when there is a tiny asymmetry.

In the finite direct coupling case, one can similarly tune the direct couplings λ_i and introduce an asymmetry to transfer the cat state into a desired cavity. This is discussed in details in

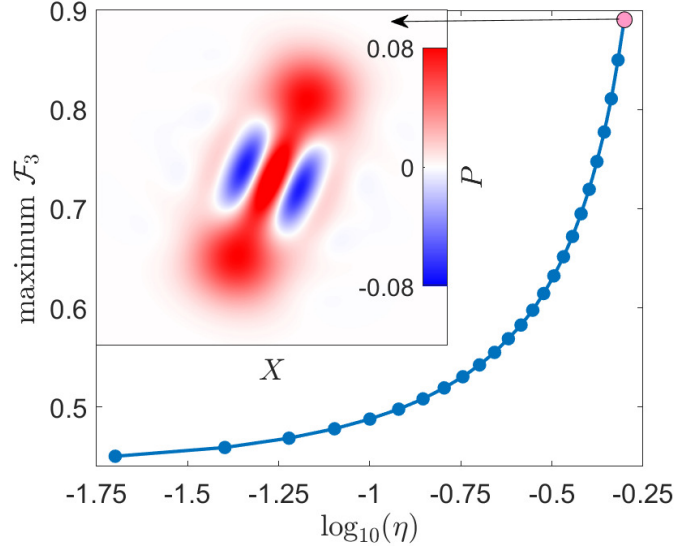


Fig. 5. Cat state transfer from 1st cavity to 3rd cavity without direct couplings ($\lambda_i = 0$). Solid curve indicates the maximum fidelity \mathcal{F}_3 achievable with the asymmetric parameter η . The inset plot is the Wigner function of the 3rd cavity when $\log_{10}(\eta) \approx -0.3$ ($\eta = 0.5$, $\delta l = 0.5$). The parameters are $\Omega_i = 1$, $\gamma = 0.1$, $\Delta = 5$,

Appendix 6.2. By tuning λ_i , similar behaviors in the classical Newton's cradle (only the balls on the ends will be lifted) can be reproduced in the quantum version analog.

6. Cat state transfer with finite direct couplings

In the previous sections, we keep our focus on the environment induced cat state transfer without direct couplings ($\lambda_i = 0$). However, the non-Markovian effect also has a significant impact in finite direct coupling cases ($\lambda_i > 0$). In this section, we will study the finite direct coupling case and show the role of non-Markovian environment in the transfer. Throughout this section, we consider the three-cavity case ($N = 3$).

6.1. Enhanced transfer by memory effect

In Fig. 6 (a), we plot the fidelity \mathcal{F}_3 of the transfer as a function of the memory time τ and the evolution time Ωt . It is shown that the cat state can be transferred into the third cavity with a large fidelity in the non-Markovian case (τ is large). As a comparison, in the Markovian case (τ is small), the fidelity of the transfer will be reduced. This is also directly reflected from the Wigner function of the transferred state in the subplots. In subplot Fig. 6 (d), the interference fringe is clear in the Wigner function, while in subplot Fig. 6 (b), the negative regions are almost invisible. It is known that the quantum superposition can be reflected by the negative regions in Wigner functions, so the shrink of the negative region in Fig. 6 (b) indicates the coherence (superposition) is partially lost. Therefore, the numerical result shows that only in the non-Markovian regime, strong coherence can be preserved in the cat state transfer. Another important feature of the non-Markovian case is the cat state can be transferred back and forth in the cavity array. In Fig. 6 (a), it is clear that the fidelity \mathcal{F}_3 has a revival when τ is large. This is the unique feature which can be only observed in non-Markovian regime. When $\tau < 1$ (close to Markovian regime), there is almost no revival. The Wigner functions plotted in subplots (c) and (e) also confirm this

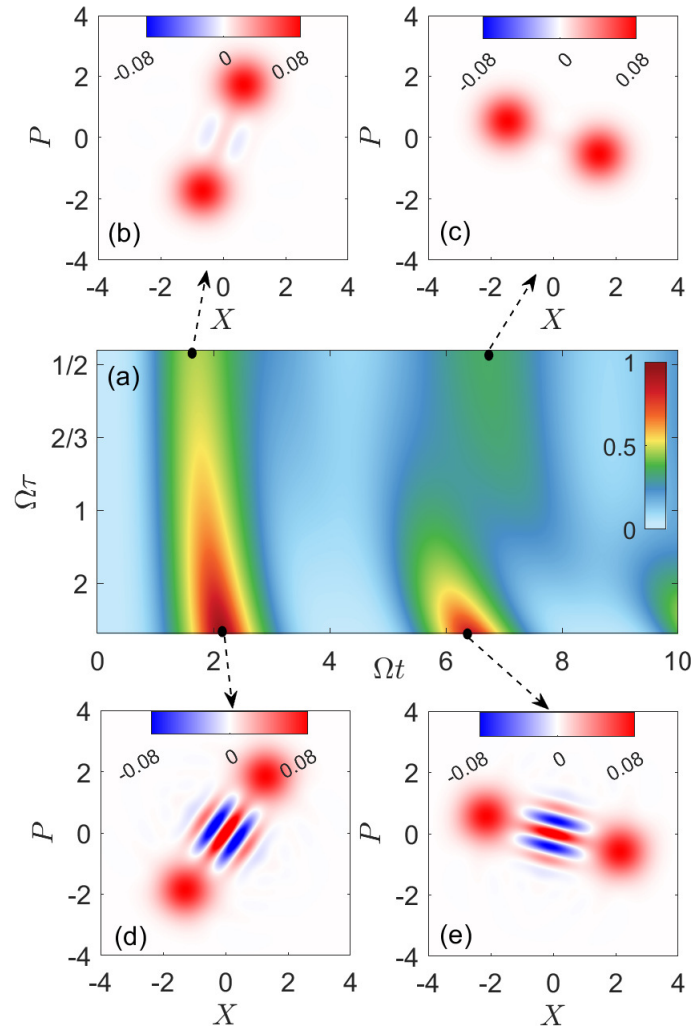


Fig. 6. Memory effect on the time evolution of the transferred fidelity \mathcal{F}_3 with finite λ_i . Subplot (a) shows \mathcal{F}_3 as a function of the memory time γ and the evolution time Ωt . Subplots (b)-(e) show the Wigner functions at the positions pointed by the arrows. The parameters are $\Omega_1 = \Omega_2 = \Omega_3 = \Omega = 1$, $\lambda_1 = \lambda_2 = 1$, $\Delta = 0$, and $\Gamma = 1$.

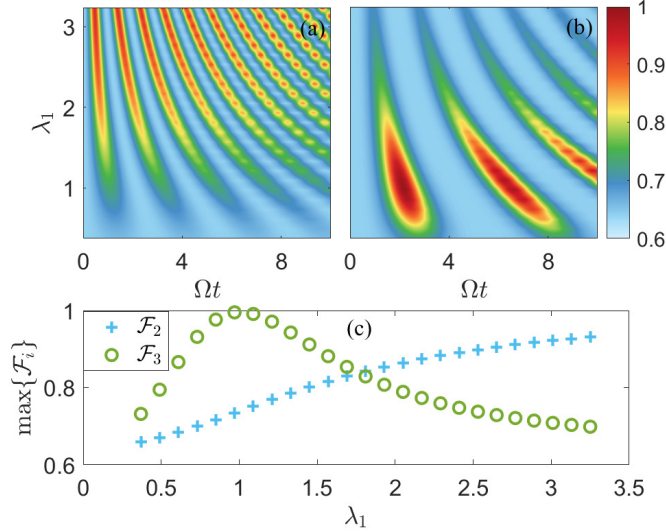


Fig. 7. (a) and (b) are the time evolution of transferred fidelities \mathcal{F}_2 and \mathcal{F}_3 , respectively. (c) is the maximum values (over Ωt) can be achieved in the time evolution as a function of λ_1 . The coupling strengths are chosen asymmetrically, while λ_2 is fixed as 1, λ_1 is varying from 0.25 to 3.25.

phenomenon. In Fig. 6 (e), negative region is clear in the Wigner function, while in Fig. 6 (c), there is no negative region at all, the coherence (superposition) is completely lost.

6.2. Asymmetric direct couplings

In the case of finite direct couplings in multiple cavities, the coupling strengths in a cavity array can be different, either because some inevitable practical factors or simply because they are intentionally tuned to be different. Interestingly, in the numerical simulation, we find the maximum transferred fidelity for the 2nd cavity and the 3rd cavity depends on the choice of the couplings. In Fig. 7, we plot the time evolution of the transferred fidelity \mathcal{F}_2 and \mathcal{F}_3 with different coupling strength λ_1 when λ_2 is fixed as 1. The value of λ_1 can be also regarded as the ratio of λ_1/λ_2 , indicating a asymmetric parameter. From Fig. 7 (a) and (b), the cat state tends to be transferred into the 2nd cavity when λ_1 is large. While λ_1 is small, the cat state is more likely to be transferred into the 3rd cavity. This is further illustrated in Fig. 7 (c), where the maximum transferred fidelity can be achieved are plotted as the function of λ_1 . It is clear that the peaks of \mathcal{F}_2 and \mathcal{F}_3 curves appear at different values of λ_1 .

To understand the impact of asymmetric couplings shown in Fig. 7, one can consider the classical Newton's cradle. The middle ball will keep stand because its position. In the quantum version of Newton's cradle, the wave function is traveling through three cavities. At each end, the wave will be reflected, forming a standing wave in the rope. For a standing wave, the amplitude at some positions can be always much smaller than the other places. The format and properties of such a “standing wave” traveling in the cavity array are certainly determined by the boundary condition and the configuration of couplings. This implies one can control the destination of the transfer in a cavity array by only tuning the coupling strength. By choosing an appropriate set of λ_i , the cat state can be precisely transferred into the desired cavity without worrying about transferring into another unwanted cavity. This mimic the behavior of classical Newton's cradle in which only the balls on the ends will be lifted.

7. Conclusion

In this manuscript, we investigate the cat state transfer in a cavity array embedded in a non-Markovian common environment. Based on the master equation derived beyond the Markovian approximation, we numerically study the cat state transfer in the cavity array. Different from traditional studies [48, 52, 53], our focus is the cat state transfer purely induced by non-Markovian environment without any directly couplings ($\lambda_i = 0$). We find that the transfer can be fundamentally different in Markovian and non-Markovian cases, reflecting by the zero or finite residue coherence. This extends the traditional understanding that non-Markovian effect only has quantitative influence (enhance or weaken) on the dynamics. The results presented here break this understanding and show the qualitative difference for Markovian and non-Markovian dynamics (can or cannot transfer cat state). This is proved analytically by pointing out the necessary condition for environment induced cat state transfer is the imaginary part of coefficient F , which only exists in non-Markovian case. We hope the results presented in the paper would be useful to the future study on cat state transfer, particularly to the investigation of the environmental impacts on the cat state transfer.

Appendix

A. Derivation of master equation

In this section, we derive the master equation from the NMQSD equation. First, we define the stochastic density operator as $P_t \equiv |\psi(t, z^*)\rangle\langle\psi(t, z)|$, the density operator is the statistical mean over all possible stochastic density operators as shown in Eq. (13). Taking the time-derivative to ρ and notice the NMQSD Eq. (8), we obtain

$$\begin{aligned} \frac{d}{dt}\rho &= \frac{d}{dt}M\{P_t\} \\ &= M\{\left[\frac{d}{dt}|\psi(t, z^*)\rangle\langle\psi(t, z)|\right]\} + M\{[|\psi(t, z^*)\rangle\langle\psi(t, z)|]\} \\ &= M\{[-iH_S + Az_t^* - A^\dagger\bar{O}]P_t\} + M\{P_t[iH_S + A^\dagger z_t - \bar{O}^\dagger A]\}. \end{aligned} \quad (21)$$

In order to compute the term $M\{Lz_t^*P_t\}$, we recall the Novikov theorem, which has been proved in Ref. [78],

$$M\{P_t z_t\} = M\{\bar{O}P_t\}, \quad (22)$$

$$M\{z_t^*P_t\} = M\{P_t\bar{O}^\dagger\}. \quad (23)$$

It is not difficult to prove the two relations above. By definition,

$$\begin{aligned} M\{P_t z_t\} &= \int \prod_k dz_k^* dz_k \exp(-\sum_k z_k^* z_k) P_t (i \sum_j g_j^* e^{-i\omega_j t} z_j) \\ &= -i \sum_j g_j^* e^{-i\omega_j t} z_j \int \prod_k dz_k^* dz_k P_t \frac{\partial}{\partial z_j^*} [\exp(-\sum_k z_k^* z_k)]. \end{aligned} \quad (24)$$

Integrating by parts, and noticing that in the polar coordinates, $[re^{-|r|^2}]_0^\infty = 0$, we obtain

$$\begin{aligned}
M\{P_t z_t\} &= i \sum_j g_j^* e^{-i\omega_j t} z_j \int \prod_k dz_k^* dz_k \frac{\partial}{\partial z_j^*} P_t \exp(-\sum_k z_k^* z_k) \\
&= i \sum_j g_j^* e^{-i\omega_j t} z_j \int \prod_k dz_k^* dz_k \left(\int ds \frac{\partial z_s^*}{\partial z_j^*} \frac{\delta}{\delta z_s^*} \right) P_t \exp(-\sum_k z_k^* z_k) \\
&= \int ds \sum_j |g_j|^2 e^{-i\omega_j(t-s)} \int \prod_k dz_k^* dz_k \exp(-\sum_k z_k^* z_k) \frac{\delta}{\delta z_s^*} P_t \\
&= \int \prod_k dz_k^* dz_k \exp(-\sum_k z_k^* z_k) \int ds K(t, s) O P_t \\
&= M\{\bar{O} P_t\}.
\end{aligned} \tag{25}$$

Similarly, one can prove

$$M\{z_t^* P_t\} = M\{P_t \bar{O}^\dagger\}. \tag{26}$$

Applying the Novikov theorem Eq. (22) and (23) to Eq. (21), we obtain the master equation as

$$\frac{d}{dt} \rho = -i[H_S, \rho] + \{[A, M\{P_t \bar{O}^\dagger\}] + h.c.\}. \tag{27}$$

In our case, the O operator derived in Eq. (10) is independent of noise variable z , $M\{P_t \bar{O}^\dagger\} = M\{P_t\} \bar{O}^\dagger = \rho \bar{O}^\dagger$ the master equation will reduce to

$$\frac{d}{dt} \rho = -i[H_S, \rho] + [A, \rho \bar{O}^\dagger] + [\bar{O} \rho, A^\dagger]. \tag{28}$$

This is the master equation (14) in the main text.

B. Master equation in finite temperature case

In the finite temperature case, the initial state of the environment is the thermal state $\rho_B(0) = \exp(-\beta H_B)/Z$, with $Z = \text{Tr}[\exp(-\beta H_B)]$ the partition function and $\beta = 1/k_B T$. According to Bose-Einstein statistics, the occupation number of the j^{th} mode is

$$\langle b_j^\dagger b_j \rangle = \bar{n}_j = \frac{1}{e^{-\beta \omega_j} - 1}. \tag{29}$$

In order to derive the master equation governing the dynamics of the cavity array system described by the Hamiltonian (1) in the finite temperature case, we introduce a fictitious environment [105]

$$H_{B'} = \sum_j \omega_j c_j^\dagger c_j,$$

where c_j is the annihilation operator of the j^{th} mode of the fictitious environment. Adding the fictitious environment without interactions with other parts, the total Hamiltonian becomes

$$H = H_S + H_B + H_{\text{int}} - H_{B'}. \tag{30}$$

Since the fictitious environment evolves independently, it has no impact on the evolution of the system. After a Bogoliubov transformation

$$b_j = \sqrt{\bar{n}_j + 1} d_j + \sqrt{\bar{n}_j} e^\dagger, \tag{31}$$

$$c_j = \sqrt{\bar{n}_j + 1} e_j + \sqrt{\bar{n}_j} d^\dagger, \quad (32)$$

the Hamiltonian becomes

$$\begin{aligned} H' = & H_S + \sum_j \omega_j d_j^\dagger d_j + \sum_j \sqrt{\bar{n}_j + 1} (g_j A d_j^\dagger + g_j^* A^\dagger d_j) \\ & - \sum_j \omega_j e_j^\dagger e_j + \sum_j \sqrt{\bar{n}_j} (g_j A e_j + g_j^* A^\dagger e_j^\dagger). \end{aligned} \quad (33)$$

It is easy to check the vacuum state for the system $|0\rangle = |0\rangle_d \otimes |0\rangle_e$ (satisfying $d_j|0\rangle = 0$, and $e_j|0\rangle = 0$) keeps the original Bose-Einstein distribution in Eq. (29) as

$$\langle 0|_d \langle 0|_e b_j^\dagger b_j |0\rangle_d |0\rangle_e = \bar{n}_j. \quad (34)$$

Therefore, the finite temperature case is mapped into a zero-temperature case with two individual environments. Solving the Hamiltonian H' with initial state $|0\rangle = |0\rangle_d \otimes |0\rangle_e$ is equivalent to solving the original Hamiltonian (1) with thermal initial state $\rho_B(0) = \exp(-\beta H_B)/Z$.

Similar to the derivation of Eq. (5), one can define $|\psi_{z,w}\rangle = \langle z, w|\psi_{\text{tot}}(t)\rangle$, where $\langle z|$ and $\langle w|$ are the coherent states of bosonic modes “ d ” and “ e ”, respectively. Then, the NMQSD equation for Hamiltonian H' is given by

$$\frac{\partial}{\partial t} |\psi_{z,w}\rangle = (-iH_S + Az_t^* + A^\dagger w_t^*) |\psi_{z,w}\rangle - A^\dagger \int_0^t ds K_1(t, s) \frac{\delta |\psi_{z,w}\rangle}{\delta z_s^*} - A \int_0^t ds K_2(t, s) \frac{\delta |\psi_{z,w}\rangle}{\delta w_s^*}, \quad (35)$$

where $z_t^* = -i \sum_j p_j z_j^* e^{i\omega_j t}$, $w_t^* = -i \sum_j q_j^* w_j^* e^{-i\omega_j t}$ are two statistically independent noises with $p_j = \sqrt{\bar{n}_j + 1} g_j$ and $q_j = \sqrt{\bar{n}_j} g_j$ as the effective coupling constants. The two Gaussian noises satisfy the following relations,

$$M[z_t] = M[z_t z_s] = 0, \quad M[z_t z_s^*] = K_1(t, s), \quad (36)$$

$$M[w_t] = M[w_t w_s] = 0, \quad M[w_t w_s^*] = K_2(t, s). \quad (37)$$

where $K_1(t, s) = \sum_j |p_j|^2 e^{-i\omega_j(t-s)}$ and $K_2(t, s) = \sum_j |q_j|^2 e^{i\omega_j(t-s)}$ are correlation functions for the two effective environments. Similar to Eq. (9), the two functional derivatives can be also replaced by two operators $O_1(t, s, z^*, w^*) |\psi_{z,w}\rangle = \frac{\delta}{\delta z_s^*} |\psi_{z,w}\rangle$ and $O_2(t, s, z^*, w^*) |\psi_{z,w}\rangle = \frac{\delta}{\delta w_s^*} |\psi_{z,w}\rangle$. According to the consistency conditions $\frac{d}{dt} \frac{\delta}{\delta z_s^*} |\psi_{z,w}\rangle = \frac{\delta}{\delta z_s^*} \frac{d}{dt} |\psi_{z,w}\rangle$ and $\frac{d}{dt} \frac{\delta}{\delta w_s^*} |\psi_{z,w}\rangle = \frac{\delta}{\delta w_s^*} \frac{d}{dt} |\psi_{z,w}\rangle$, the operators O_1 and O_2 should satisfy the following equations

$$\frac{\partial}{\partial t} O_1 = [-iH_S + Az_t^* + A^\dagger w_t^* - A^\dagger \bar{O}_1 - A \bar{O}_2, O_1] - A^\dagger \frac{\delta}{\delta z_s^*} \bar{O}_1 - A \frac{\delta}{\delta z_s^*} \bar{O}_2, \quad (38)$$

$$\frac{\partial}{\partial t} O_2 = [-iH_S + Az_t^* + A^\dagger w_t^* - A^\dagger \bar{O}_1 - A \bar{O}_2, O_2] - A^\dagger \frac{\delta}{\delta w_s^*} \bar{O}_1 - A \frac{\delta}{\delta w_s^*} \bar{O}_2. \quad (39)$$

where $\bar{O}_i = \int_0^t K_i(t, s) O_i(t, s, z^*, w^*) ds$ ($i = 1, 2$). According to Eqs. (38-39), the exact O operators for the N -cavity model can be determined as

$$O_1(t, s, w^*) = \sum_{i=1}^N x_i(t, s) a_i + \int_0^t x'(t, s, s') w_{s'}^* ds', \quad (40)$$

$$O_2(t, s, z^*) = \sum_{i=1}^N y_i(t, s) a_i^\dagger + \int_0^t y'(t, s, s') z_{s'}^* ds', \quad (41)$$

while the coefficients satisfy the following equations

$$\begin{aligned} \frac{\partial}{\partial t} x_i(t, s) = & i\Omega_i x_i(t, s) + i[\lambda_i x_{i+1}(t, s) + \lambda_{i-1} x_{i-1}(t, s)] \\ & + \sum_{j=1}^N x_j(t, s)[Y_j(t) + X_i(t)] - Y'(t, s), \end{aligned} \quad (42)$$

$$\begin{aligned} \frac{\partial}{\partial t} y_i(t, s) = & -i\Omega_i y_i(t, s) - i[\lambda_i y_{i+1}(t, s) + \lambda_{i-1} y_{i-1}(t, s)] \\ & - \sum_{j=1}^N y_j(t, s)X_j(t) - \sum_{j=1}^N y_j(t, s)Y_i(t) - X'(t, s), \end{aligned} \quad (43)$$

$$\frac{\partial}{\partial t} x'(t, s, s') = \sum_{j=1}^N x_j(t, s)X'(t, s'), \quad (44)$$

$$\frac{\partial}{\partial t} y'(t, s, s') = - \sum_{j=1}^N y_j(t, s)Y'(t, s'), \quad (45)$$

where $X_i(t) = \int_0^t K_1(t, s)x_i(t, s)ds$, $X'(t, s') = \int_0^t K_1(t, s)x'(t, s, s')ds$, $Y_i(t) = \int_0^t K_2(t, s)y_i(t, s)ds$, and $Y'(t, s') = \int_0^t K_2(t, s)y'(t, s, s')ds$, with the initial conditions $x_i(t, t) = 1$, $y_i(t, t) = 1$, $x'(t, t, s') = y'(t, t, s') = 0$, $x'(t, s, t) = -\sum_{j=1}^N x_j(t, s)$, and $y'(t, s, t) = \sum_{j=1}^N y_j(t, s)$. With the O operators and the coefficients in Eqs. (40-45), one can numerically simulate the evolution of the cavity array in finite temperature case by using Eq. (35). Certainly, a master equation can be also obtained by following the method in Refs. [106, 107].

The numerical results (not presented) show the temperature effect can enhance or weaken the transfer. However, in this paper, we focus on some distinctive difference between non-Markovian and Markovian environments. Instead of “enhance or weaken”, we pay more attention to “can or cannot”. The detailed influence of the temperature can be investigated elsewhere in the future.

Funding.

National Natural Science Foundation of China under Grant Nos. 62471143 and 11874114
 Natural Science Funds for Distinguished Young Scholar of Fujian Province under Grant 2020J06011
 Natural Science Foundation of Fujian Province under Grant No. 2022J01548
 Project from Fuzhou University under Grant No. JG202001-2 and Grant No. GXRC-21014.

Acknowledgments. This work was supported by the National Natural Science Foundation of China under Grant Nos. 62471143 and 11874114, the Natural Science Funds for Distinguished Young Scholar of Fujian Province under Grant 2020J06011, Natural Science Foundation of Fujian Province under Grant No. 2022J01548, Project from Fuzhou University under Grant No. JG202001-2 and Grant No. GXRC-21014.

Disclosures. The authors declare no conflicts of interest.

References

1. E. Schrödinger, “Die gegenwärtige situation in der quantenmechanik,” *Naturwissenschaften* **23**, 807–812 (1935).
2. C. Monroe, D. M. Meekhof, B. E. King, and D. J. Wineland, “A “schrodinger cat” superposition state of an atom,” *Science* **272**, 1131–1136 (1996).
3. W. H. Zurek, “Decoherence and the transition from quantum to classical,” *Phys. Today* **44**, 36–44 (1991).
4. W. H. Zurek, “Decoherence, einselection, and the quantum origins of the classical,” *Rev. Mod. Phys.* **75**, 715–775 (2003).
5. M. Schlosshauer, “Quantum decoherence,” *Phys. Rep.* **831**, 1–57 (2019).
6. J. M. Raimond, M. Brune, and S. Haroche, “Reversible decoherence of a mesoscopic superposition of field states,” *Phys. Rev. Lett.* **79**, 1964–1967 (1997).

7. S. Haroche, “Quantum information with atoms and photons in a cavity: Entanglement, complementarity and decoherence studies,” *Phys. Scr.* **T102**, 128 (2002).
8. J. M. Raimond, M. Brune, and S. Haroche, “Manipulating quantum entanglement with atoms and photons in a cavity,” *Rev. Mod. Phys.* **73**, 565–582 (2001).
9. L. Pezzè, M. Gessner, P. Feldmann, *et al.*, “Heralded generation of macroscopic superposition states in a spinor bose-einstein condensate,” *Phys. Rev. Lett.* **123**, 260403 (2019).
10. F.-Y. Zhang and C.-P. Yang, “Generation of generalized hybrid entanglement in cavity electro-optic systems,” *Quantum Sci. Technol.* **6**, 025003 (2021).
11. Z. Wang, Z. Bao, Y. Wu, *et al.*, “A flying schrödinger’s cat in multipartite entangled states,” *Sci. Adv.* **8** (2022).
12. F.-X. Sun, S.-S. Zheng, Y. Xiao, *et al.*, “Remote generation of magnon schrödinger cat state via magnon-photon entanglement,” *Phys. Rev. Lett.* **127**, 087203 (2021).
13. Y.-H. Chen, W. Qin, X. Wang, *et al.*, “Shortcuts to adiabaticity for the quantum rabi model: Efficient generation of giant entangled cat states via parametric amplification,” *Phys. Rev. Lett.* **126**, 023602 (2021).
14. Y.-H. Chen, W. Qin, R. Stassi, *et al.*, “Fast binomial-code holonomic quantum computation with ultrastrong light-matter coupling,” *Phys. Rev. Res.* **3**, 033275 (2021).
15. S. Haroche, M. Brune, and J.-M. Raimond, “Schrödinger cat states and decoherence studies in cavity qed,” *Eur. Phys. J. Special Top.* **159**, 19–26 (2008).
16. F. Assemat, D. Grossi, A. Signoles, *et al.*, “Quantum rabi oscillations in coherent and in mesoscopic cat field states,” *Phys. Rev. Lett.* **123**, 143605 (2019).
17. S. D. Du, S. Q. Gong, Z. Z. Xu, *et al.*, “Production of two-mode optical schrodinger catlike states via kerr nonlinearity,” *Opt. Commun.* **138**, 193–199 (1997).
18. H. C. Fu and A. I. Solomon, “Kerr cat states from the four-photon jaynes-cummings model,” *J. Mod. Opt.* **49**, 259–268 (2002).
19. A. Grimm, N. E. Frattini, S. Puri, *et al.*, “Stabilization and operation of a kerr-cat qubit,” *Nature* **584**, 205–+ (2020).
20. M. G. A. Paris, “Generation of mesoscopic quantum superpositions through kerr-stimulated degenerate downconversion,” *J. Opt. B: Quantum Semiclass. Opt.* **1**, 662–667 (1999).
21. P. Zapletal, A. Nunnenkamp, and M. Brunelli, “Stabilization of multimode schrodinger cat states via normal-mode dissipation engineering,” *PRX Quantum* **3**, 010301 (2022).
22. D. Xu, X.-K. Gu, H.-K. Li, *et al.*, “Quantum control of a single magnon in a macroscopic spin system,” *Phys. Rev. Lett.* **130**, 193603 (2023).
23. Y. A. Yang, W.-T. Luo, J.-L. Zhang, *et al.*, “Minute-scale schrödinger-cat state of spin-5/2 atoms,” *Nat. Photonics* (2024).
24. M. Cosacchi, T. Seidelmann, J. Wiercinski, *et al.*, “Schrodinger cat states in quantum-dot-cavity systems,” *Phys. Rev. Res.* **3**, 023088 (2021).
25. M. Bild, M. Fadel, Y. Yang, *et al.*, “Schrödinger cat states of a 16-microgram mechanical oscillator,” *Science* **380**, 274–278 (2023).
26. O. Romero-Isart, M. L. Juan, R. Quidant, and J. I. Cirac, “Toward quantum superposition of living organisms,” *New J. Phys.* **12**, 033015 (2010).
27. A. S. Darmawan, B. J. Brown, A. L. Grimsmo, *et al.*, “Practical quantum error correction with the xzzx code and kerr-cat qubits,” *PRX Quantum* **2**, 030345 (2021).
28. H. Goto, Z. R. Lin, T. Yamamoto, and Y. Nakamura, “On-demand generation of traveling cat states using a parametric oscillator,” *Phys. Rev. A* **99**, 023838 (2019).
29. M. J. Kewming, S. Shrapnel, and G. J. Milburn, “Quantum correlations in the kerr ising model,” *New J. Phys.* **22** (2020).
30. S. Puri, S. Boutin, and A. Blais, “Engineering the quantum states of light in a kerr-nonlinear resonator by two-photon driving,” *Npj Quantum Inf.* **3**, 18 (2017).
31. Q. Xu, J. K. Iverson, F. G. S. L. Brandao, and L. Jiang, “Engineering fast bias-preserving gates on stabilized cat qubits,” *Phys. Rev. Res.* **4**, 013082 (2022).
32. Y.-H. Chen, Z.-C. Shi, F. Nori, and Y. Xia, “Error-tolerant amplification and simulation of the ultrastrong-coupling quantum rabi model,” *Phys. Rev. Lett.* **133**, 033603 (2024).
33. Z.-Y. Zhou, C. Gneiting, W. Qin, *et al.*, “Enhancing dissipative cat-state generation via nonequilibrium pump fields,” *Phys. Rev. A* **106**, 023714 (2022).
34. W. Qin, A. Miranowicz, H. Jing, and F. Nori, “Generating long-lived macroscopically distinct superposition states in atomic ensembles,” *Phys. Rev. Lett.* **127**, 093602 (2021).
35. Z.-Y. Zhou, C. Gneiting, J. Q. You, and F. Nori, “Generating and detecting entangled cat states in dissipatively coupled degenerate optical parametric oscillators,” *Phys. Rev. A* **104**, 013715 (2021).
36. Y.-H. Kang, Y.-H. Chen, X. Wang, *et al.*, “Nonadiabatic geometric quantum computation with cat-state qubits via invariant-based reverse engineering,” *Phys. Rev. Res.* **4**, 013233 (2022).
37. H.-Y. Ku, N. Lambert, F.-J. Chan, *et al.*, “Experimental test of non-macrorealistic cat states in the cloud,” *npj Quantum Inf.* **6** (2020).
38. X. Wang, A. Miranowicz, H.-R. Li, and F. Nori, “Hybrid quantum device with a carbon nanotube and a flux qubit for dissipative quantum engineering,” *Phys. Rev. B* **95**, 205415 (2017).
39. A. L. Grimsmo, J. Combes, and B. Q. Baragiola, “Quantum computing with rotation-symmetric bosonic codes,”

Phys. Rev. X **10**, 011058 (2020).

40. A. P. Lund, T. C. Ralph, and H. L. Haselgrove, “Fault-tolerant linear optical quantum computing with small-amplitude coherent states,” Phys. Rev. Lett. **100**, 030503 (2008).
41. M. Mirrahimi, Z. Leghtas, V. V. Albert, *et al.*, “Dynamically protected cat-qubits: a new paradigm for universal quantum computation,” New J. Phys. **16**, 045014 (2014).
42. Z. Ni, S. Li, X. Deng, *et al.*, “Beating the break-even point with a discrete-variable-encoded logical qubit,” Nature **616**, 56–60 (2023).
43. S. Chao, B. Xiong, and L. Zhou, “Generating a squeezed-coherent-cat state in a double-cavity optomechanical system,” Ann. Phys. **531** (2019).
44. B. Xiong, X. Li, S.-L. Chao, *et al.*, “Generation of entangled schrödinger cat state of two macroscopic mirrors,” Opt. Express **27**, 13547 (2019).
45. Z. Yang, S.-L. Chao, and L. Zhou, “Generating macroscopic quantum superposition and a phonon laser in a hybrid optomechanical system,” J. Opt. Soc. Am. B **37**, 1 (2019).
46. X. L. He, Z. F. Zheng, Y. Zhang, and C. P. Yang, “One-step transfer of quantum information for a photonic cat-state qubit,” Quantum Inf. Process. **19**, 80 (2020).
47. H. Jeong and T. C. Ralph, “Transfer of nonclassical properties from a microscopic superposition to macroscopic thermal states in the high temperature limit,” Phys. Rev. Lett. **97**, 100401 (2006).
48. T. Liu, Z. F. Zheng, Y. Zhang, *et al.*, “Transferring entangled states of photonic cat-state qubits in circuit qed,” Front. Phys. **15**, 21603 (2020).
49. D. Ran, C. S. Hu, and Z. B. Yang, “Entanglement transfer from two-mode continuous variable su(2) cat states to discrete qubits systems in jaynes-cummings dimers,” Sci. Rep. **6**, 32089 (2016).
50. X. Zhao, P. Huang, and X. Hu, “Doppler effect induced spin relaxation boom,” Sci. Rep. **6**, 23169 (2016).
51. X. Zhao and X. Hu, “Toward high-fidelity coherent electron spin transport in a gaas double quantum dot,” Sci. Rep. **8**, 13968 (2018).
52. Y. X. Zeng, J. Shen, M. S. Ding, and C. Li, “Macroscopic schrodinger cat state swapping in optomechanical system,” Opt. Express **28**, 9587–9602 (2020).
53. Z. Feng, Z.-W. Gao, L.-A. Wu, *et al.*, “Photonic newton’s cradle for remote energy transport,” Phys. Rev. Appl. **11**, 044009 (2019).
54. V. V. Dodonov, M. A. Andreata, and S. S. Mizrahi, “Decoherence and transfer of quantum states of field modes in a one-dimensional cavity with an oscillating boundary,” J. Opt. B: Quantum Semiclass. Opt. **7**, S468–S479 (2005).
55. J. Lidal and J. Danon, “Generation of schrodinger-cat states through photon-assisted landau-zener-stuckelberg interferometry,” Phys. Rev. A **102**, 043717 (2020).
56. T. Prudencio, “Quantum state transfer and hadamard gate for coherent states,” Int. J. Quantum Inf. **11**, 1350024 (2013).
57. R. Y. Teh, S. Kiesewetter, P. D. Drummond, and M. D. Reid, “Creation, storage, and retrieval of an optomechanical cat state,” Phys. Rev. A **98**, 063814 (2018).
58. C. Gauld and R. Cross, “Understanding newton’s cradle. i: modelling the ideal cradle,” Phys. Educ. **56**, 025001 (2020).
59. R. Cross, “Edme mariotte and newton’s cradle,” The Phys. Teach. **50**, 206–207 (2012).
60. C. F. Gauld, “Newton’s cradle in physics education,” Sci. Educ. **15**, 597–617 (2006).
61. H.-P. Breuer, E.-M. Laine, and J. Piilo, “Measure for the degree of non-markovian behavior of quantum processes in open systems,” Phys. Rev. Lett. **103**, 210401 (2009).
62. B.-H. Liu, L. Li, Y.-F. Huang, *et al.*, “Experimental control of the transition from markovian to non-markovian dynamics of open quantum systems,” Nat. Phys. **7**, 931–934 (2011).
63. B. Bellomo, R. Lo Franco, and G. Compagno, “Non-markovian effects on the dynamics of entanglement,” Phys. Rev. Lett. **99**, 160502 (2007).
64. K. L. Liu and H. S. Goan, “Non-markovian entanglement dynamics of quantum continuous variable systems in thermal environments,” Phys. Rev. A **76**, 022312 (2007).
65. R. Lo Franco, B. Bellomo, S. Maniscalco, and G. Compagno, “Dynamics of quantum correlations in two-qubit systems within non-markovian environments,” Internat. J. Mod. Phys. B **27**, 1345053 (2013).
66. H.-P. Breuer, E.-M. Laine, J. Piilo, and B. Vacchini, “Colloquium: Non-markovian dynamics in open quantum systems,” Rev. Mod. Phys. **88**, 021002 (2016).
67. T. Yu and J. H. Eberly, “Finite-time disentanglement via spontaneous emission,” Phys. Rev. Lett. **93**, 140404 (2004).
68. T. Yu and J. H. Eberly, “Sudden death of entanglement,” Science **323**, 598–601 (2009).
69. J.-Q. Liao, Z. R. Gong, L. Zhou, *et al.*, “Controlling the transport of single photons by tuning the frequency of either one or two cavities in an array of coupled cavities,” Phys. Rev. A **81**, 042304 (2010).
70. N. Meher, S. Sivakumar, and P. K. Panigrahi, “Duality and quantum state engineering in cavity arrays,” Sci. Rep. **7** (2017).
71. D. Dubyna and W. Kuo, “Inter-qubit interaction mediated by collective modes in a linear array of three-dimensional cavities,” Quantum Sci. Technol. **5**, 035002 (2020).
72. A. Saxena, A. Manna, R. Trivedi, and A. Majumdar, “Realizing tight-binding hamiltonians using site-controlled coupled cavity arrays,” Nat. Commun. **14** (2023).
73. J. Q. You and F. Nori, “Atomic physics and quantum optics using superconducting circuits,” Nature **474**, 589–597

(2011).

74. J. H. An and W. M. Zhang, “Non-markovian entanglement dynamics of noisy continuous-variable quantum channels,” *Phys. Rev. A* **76**, 042127 (2007).
75. L. Diósi and W. T. Strunz, “The non-markovian stochastic schrodinger equation for open systems,” *Phys. Lett. A* **235**, 569–573 (1997).
76. L. Diósi, N. Gisin, and W. T. Strunz, “Non-markovian quantum state diffusion,” *Phys. Rev. A* **58**, 1699–1712 (1998).
77. W. T. Strunz, L. Diósi, and N. Gisin, “Open system dynamics with non-markovian quantum trajectories,” *Phys. Rev. Lett.* **82**, 1801–1805 (1999).
78. T. Yu, L. Diósi, N. Gisin, and W. T. Strunz, “Non-markovian quantum-state diffusion: Perturbation approach,” *Phys. Rev. A* **60**, 91–103 (1999).
79. X. Zhao, J. Jing, B. Corn, and T. Yu, “Dynamics of interacting qubits coupled to a common bath: Non-markovian quantum-state-diffusion approach,” *Phys. Rev. A* **84**, 032101 (2011).
80. X. Zhao, W. Shi, L.-A. Wu, and T. Yu, “Fermionic stochastic schrodinger equation and master equation: An open-system model,” *Phys. Rev. A* **86**, 032116 (2012).
81. X. Zhao, W. Shi, J. Q. You, and T. Yu, “Non-markovian dynamics of quantum open systems embedded in a hybrid environment,” *Ann. Phys.* **381**, 121–136 (2017).
82. X. Zhao, “Macroscopic entanglement in optomechanical system induced by non-markovian environment,” *Opt. Express* **27**, 29082–29097 (2019).
83. D.-W. Luo and T. Yu, “Geometric signature of non-markovian dynamics,” (2023).
84. W. Shi, Y. Chen, Q. Ding, *et al.*, “Positivity-preserving non-markovian master equation for open quantum system dynamics: Stochastic schrödinger equation approach,” *Phys. Rev. A* **109**, 022203 (2024).
85. D.-W. Luo, X.-F. Qian, and T. Yu, “Optically mediated remote entanglement generation in magnon-cavity systems,” *Phys. Rev. A* **109**, 012611 (2024).
86. L. Chen, D. I. G. Bennett, and A. Eisfeld, “Calculating nonlinear response functions for multidimensional electronic spectroscopy using dyadic non-markovian quantum state diffusion,” *J. Chem. Phys.* **157**, 114104 (2022).
87. S. Flannigan, F. Damanet, and A. J. Daley, “Many-body quantum state diffusion for non-markovian dynamics in strongly interacting systems,” *Phys. Rev. Lett.* **128**, 063601 (2022).
88. S.-f. Qi and J. Jing, “Magnon-mediated quantum battery under systematic errors,” *Phys. Rev. A* **104**, 032606 (2021).
89. X. Turkeshi, A. Biella, R. Fazio, *et al.*, “Measurement-induced entanglement transitions in the quantum ising chain: From infinite to zero clicks,” *Phys. Rev. B* **103**, 224210 (2021).
90. F.-H. Ren, Z.-M. Wang, and L.-A. Wu, “Accelerated adiabatic quantum search algorithm via pulse control in a non-markovian environment,” *Phys. Rev. A* **102**, 062603 (2020).
91. Z.-M. Wang, F.-H. Ren, D.-W. Luo, *et al.*, “Almost-exact state transfer by leakage-elimination-operator control in a non-markovian environment,” *Phys. Rev. A* **102**, 042406 (2020).
92. K. Luoma, W. T. Strunz, and J. Piilo, “Diffusive limit of non-markovian quantum jumps,” *Phys. Rev. Lett.* **125**, 150403 (2020).
93. Y.-H. Ma, Q.-Z. Ding, and T. Yu, “Persistent spin squeezing of a dissipative one-axis twisting model embedded in a general thermal environment,” *Phys. Rev. A* **101**, 022327 (2020).
94. X. Gao and A. Eisfeld, “Charge and energy transfer in large molecular assemblies: Quantum state diffusion with an adaptive basis,” *J. Chem. Phys.* **150**, 234115 (2019).
95. V. Link, K. Luoma, and W. T. Strunz, “Revealing the nature of nonequilibrium phase transitions with quantum trajectories,” *Phys. Rev. A* **99**, 062120 (2019).
96. X. Zhao, Y.-h. Ma, and Y. Xia, “Noise-assisted quantum coherence protection in a hierarchical environment,” *Phys. Rev. A* **105**, 042217 (2022).
97. J. Dalibard, Y. Castin, and K. Mølmer, “Wave-function approach to dissipative processes in quantum optics,” *Phys. Rev. Lett.* **68**, 580–583 (1992).
98. N. Gisin and I. C. Percival, “Quantum state diffusion, localization and quantum dispersion entropy,” *J. Phys. A-math. Gen.* **26**, 2233–2243 (1993).
99. Q. Mu, X. Zhao, and T. Yu, “Memory-effect-induced macroscopic-microscopic entanglement,” *Phys. Rev. A* **94**, 012334 (2016).
100. M. W. Y. Tu and W.-M. Zhang, “Non-markovian decoherence theory for a double-dot charge qubit,” *Phys. Rev. B* **78**, 235311 (2008).
101. W. Shi, X. Zhao, and T. Yu, “Non-markovian fermionic stochastic schrodinger equation for open system dynamics,” *Phys. Rev. A* **87**, 052127 (2013).
102. L. Diósi, “Non-markovian continuous quantum measurement of retarded observables,” *Phys. Rev. Lett.* **100**, 080401 (2008).
103. H. M. Wiseman and J. M. Gambetta, “Pure-state quantum trajectories for general non-markovian systems do not exist,” *Phys. Rev. Lett.* **101**, 140401 (2008).
104. J. H. Eberly and T. Yu, “The end of an entanglement,” *Science* **316**, 555–557 (2007).
105. T. Yu, “Non-markovian quantum trajectories versus master equations: Finite-temperature heat bath,” *Phys. Rev. A* **69**, 062107 (2004).
106. Y. Chen, J. Q. You, and T. Yu, “Exact non-markovian master equations for multiple qubit systems: Quantum-trajectory approach,” *Phys. Rev. A* **90**, 052104 (2014).

107. W. T. Strunz and T. Yu, “Convolutionless non-markovian master equations and quantum trajectories: Brownian motion,” *Phys. Rev. A* **69**, 052115 (2004).